

## THE USE OF FIELD INDENTATION MICROPROBE IN MEASURING MECHANICAL PROPERTIES OF WELDS

**F. M. Haggag, H. Wong, D. J. Alexander, R. K. Nanstad**

Metals and Ceramics Division  
Oak Ridge National Laboratory  
P. O. Box 2008  
Oak Ridge, TN 37831-6151, USA

### ABSTRACT

A field indentation microprobe (FIM) was conceived for evaluating the structural integrity of metallic components (including base metal, welds, and heat-affected zones) in situ in a nondestructive manner. The FIM consists of an automated ball indentation (ABI) unit for determining the mechanical properties (yield strength, flow properties, estimates of fracture toughness, etc.) and a nondestructive evaluation (NDE) unit (consisting of ultrasonic transducers and a video camera) for determining the physical properties such as crack size, material pile-up around indentation, and residual stress presence and orientation. The laboratory version used in this work performs only ABI testing.

ABI tests were performed on stainless steel base metal (type 316L), heat-affected-zone, and welds (type 308). Excellent agreement was obtained between yield strength and flow properties (true-stress/true-plastic-strain curve) measured by the ABI tests and those from uniaxial tensile tests conducted on 308 stainless steel welds, thermally aged at 343°C for different times, and on the base material.

### INTRODUCTION

To assess the integrity of structures following accidents or severe service conditions, knowledge of the material's mechanical properties, the size and extent of induced defects, and the current thickness and residual stresses are required. This is particularly important for welds as well as base materials and heat-affected zones. This was one incentive to develop a nondestructive testing apparatus such as the FIM which described in detail in Ref. 1 and briefly presented here (together with ABI test results on 308 stainless steel welds). Other motivations are its

general applications as the in-service examination of components, welding characterizations, new alloy development, and when limited amounts of material are available.

### THE FIELD INDENTATION MICROPROBE (FIM)

The main components of the FIM apparatus are shown schematically in Fig. 1. The method of mounting the testing head of the FIM on the structural component is not shown since the exact mechanism will vary on a case-to-case basis depending upon the geometry and position of the particular structure. A tripod arrangement, for example, facilitates adjustment of the ball indenter to be perpendicular to the surface of the structure or test specimen. The load can be applied by hydraulic, pneumatic, mechanical, or any other means. The FIM consists of two main units: an automated ball indentation (ABI) unit for measuring the mechanical properties and a nondestructive evaluation (NDE) unit (consisting of ultrasonic transducers and a video camera) for determining the physical properties such as crack size, material pile-up around indentation, and residual stress presence and orientation.

The mechanical properties determined by the FIM apparatus include elastic modulus, yield strength, Lüders strain, strain-hardening exponent, true-stress/true-plastic-strain curve up to 20% strain, and residual stress presence and orientation. The fracture toughness can be estimated using the ABI measured flow properties and a modified critical fracture strain model as discussed in Ref. 2. Furthermore, the shift in the ductile-to-brittle transition temperature for ferritic steel plates and welds, e.g., due to the neutron irradiation embrittlement, can be estimated from the ABI-measured change in the material yield strength. ABI tests were conducted successfully on unirradiated and irradiated A212 grade B pressure vessel steel (Ref. 3).

## THE AUTOMATED BALL INDENTATION (ABI) TEST

The ABI test is based on multiple indentation (at the same penetration location) of a polished metallic surface by a spherical indenter. This is accomplished by cyclic loading and unloading of the spherical indenter into the test material where the load is increased in the successive loading cycles. The applied loads and associated displacements (depth of penetration of the indenter into the test specimen) are measured during both loading and unloading using a load cell and a linear variable differential transducer (LVDT). The test set-up of the current work used a 0.76-mm-diam (0.030-in.) ball indenter and a spring-loaded LVDT which were mounted to the load cell of an MTS hydraulic testing machine. Details of the ball indenter and the LVDT are shown in Fig. 2. An in-house data acquisition and control system and a Hewlett-Packard computer were used for automated testing as well as acquiring and processing test data. The load-displacement data were used to determine the yield strength and produce the ABI-derived true-stress/true-plastic-strain curve. The ABI analyses are based primarily on elasticity and plasticity theories and some empirical correlations as described in Refs. 1 and 3. The primary equations used in these analyses are given in the next section. This paper presents ABI test results on aged stainless steel welds.

## MATERIALS AND TEST PROCEDURE

The primary materials chosen here for conducting the ABI tests were three different 308 stainless steel (SS) welds. The base metal for all the welds was 25-mm-thick (1-in.) 304L stainless steel plate. The filler metal composition was adjusted to result in ferrite numbers of 4, 8, and 12. The welds were aged at 343° C in an air atmosphere for 3,000, 10,000, and 20,000 h. Details of other mechanical properties (e.g., Charpy V-notch impact test results) as well as discussion of the thermal embrittlement mechanism for these aged welds are presented in another paper of this conference (Ref. 4).

Indentation tests were conducted, at room temperature, on the top and bottom of these 308 SS weld specimens in the as-welded and aged conditions. The geometry of laboratory specimens for valid ABI testing must satisfy thickness and area requirements around the final indentation relative to the size of the indenter. However, for actual field applications these requirements will be satisfied for most structural components. All 12 welds tested here met the

geometry requirements for valid ABI tests since each weld was a block of approximately 25 mm thick, 50 mm wide (base metal and weld), and 50 mm long with the weld area being approximately 25 mm wide at the top and 13 mm wide at the bottom.

Schematics of the ABI load-displacement (indentation depth) plot and the profile of indentation (exaggerated to show material pile-up) are shown in Figs. 3 and 4. The FIM analyses use an innovative method for analyzing the load-displacement data to determine the yield strength and to produce the true-stress/true-plastic-strain curve as explained below (Refs. 1 and 3). After the testing head is properly secured to the structure so that the load cell is perpendicular to the surface, the surface is prepared using the polishing tool. Thereafter, the computer causes the indenter tip to be brought into contact with the polished surface. The total and plastic indentation depths ( $h_{t1}$  and  $h_{p1}$ ) and applied indentation load ( $P_1$ ) are then measured for the first cycle. Typically the load is increased for each succeeding cycle and the values of  $P$ ,  $h_t$ , and  $h_p$  are measured for each cycle. Several load cycles (typically five or more) are conducted at the same indentation location for determining a full true-stress/true-plastic-strain curve at this location (data from each cycle yield a point on this curve). This cyclic loading can be continued; however, the maximum total indentation depth ( $h_t$ ) should not exceed one-half the diameter,  $D$ , of the indenter. Following the final cycle the plastic indentation diameter,  $d_p$ , can be independently measured using the video camera. As stated above, the FIM operation is typically controlled by a program stored in the computer, and data as to the load, indentation depth, etc., measured using the data acquisition system are stored on magnetic discs in the computer for post-test processing.

## ABI DATA ANALYSIS

The homogeneous plastic flow portion of the true-stress ( $\sigma_t$ )/true-plastic-strain ( $\epsilon_p$ ) curve can be represented by the familiar power law equation:

$$\sigma_t = K \epsilon_p^n \quad (1)$$

where

$n$  = strain-hardening exponent

$K$  = strength coefficient.

It should be noted that this representation is not a necessary requirement for determining the indentation derived  $\sigma_t - \epsilon_p$  data as will be shown later (equations 2 and 3), but it can be used to determine the strain-hardening exponent over the  $\epsilon_p$  range of interest. Furthermore, a single power curve may not fit the entire  $\sigma_t - \epsilon_p$  curve as noted in ASTM Standard E-646-78.

A computer program is used to solve the following

equations and to thereby determine the flow curve from the ABI data.

$$\epsilon_p = 0.2 d_p/D \quad (2)$$

$$\sigma_t = 4P/\pi d_p^2 \delta \quad (3)$$

where

$$d_p = \{9.5 CD [h_p^2 + (d_p/2)^2] / [h_p^2 + (d_p/2)^2 - h_p D]\}^{1/3} \quad (4)$$

$$C = 5.47P(1/E_1 + 1/E_2) \quad (5)$$

$$\delta = \begin{cases} 1.12 & \phi \leq 1 \\ 1.12 + \tau \ln \phi & 1 < \phi \leq 27 \\ \delta_{\max} & \phi > 27 \end{cases} \quad (6)$$

$$\phi = \epsilon_p E_2 / 0.43 \sigma_t \quad (7)$$

$$\delta_{\max} = 2.87 \alpha_m \quad (8)$$

$$\tau = (\delta_{\max} - 1.12) / \ln(27) \quad (9)$$

In the above equations,  $\sigma_t$  is the true stress,  $\epsilon_p$  is the true-plastic-strain,  $d_p$  is the plastic indentation diameter,  $D$  is the diameter of the ball indenter,  $P$  is the applied indentation load,  $h_p$  is the plastic indentation depth,  $E_1$  is the elastic modulus of the indenter,  $E_2$  is the elastic modulus of the test material,  $\delta$  is the parameter whose value depends on the stage of development of the plastic zone beneath of the indenter,  $\alpha_m$  is a parameter proportional to the strain rate sensitivity of the test material or specimen (e.g., for low strain-rate-sensitive materials  $\alpha_m = 1.0$ ), and  $\ln$  is the natural logarithm.

The computer program is used to fit the ABI-derived  $\sigma_t$ - $\epsilon_p$  data (calculated using equations 2 and 3) by linear regression analysis to the relationship of equation 1, and determine the strain-hardening exponent ( $n$ ) and the strength coefficient ( $K$ ). The previous equations provide means for predicting the homogeneous portion of the stress/strain curve from indentation data.

A different approach must be used for measuring the yield strength. For each ABI loading cycle the total penetration depth ( $h_t$ ) is measured while the load is being applied, then converted to a total indentation diameter ( $d_t$ ) using the following equation:

$$d_t = 2 (h_t D - h_t^2)^{0.5} \quad (10)$$

Data points from all loading cycles up to  $d_t/D = 1.0$  are fit by linear regression analysis to the following relationship:

$$P/d_t^2 = A (d_t/D)^{m-2} \quad (11)$$

where  $P$  is the applied indentation load,  $m$  is Meyer's coefficient, and  $A$  is a test material (or specimen) parameter obtained from the regression analysis of test data of  $d_t/D$  versus  $P/d_t^2$ . The test material parameter ( $A$ ) is then used to calculate the yield strength ( $\sigma_y$ ) of the material using the following equation:

$$\sigma_y = \beta_m A \quad (12)$$

where  $\beta_m$  is a material-type constant (e.g., a single

value of  $\beta_m = 0.2285$  is applicable to all carbon steels whether cold rolled, hot rolled, or irradiated). The value of  $\beta_m$  for each class or type of material is determined from regression analysis of various tensile yield-strength values and their corresponding "A" values as measured from entire ABI curves (up to  $d_t/D = 1.0$ ). In equation 12 above, the units of  $A$  and  $\sigma_y$  should be the same.

## ABI RESULTS AND DISCUSSION

For each loading cycle the total penetration depth ( $h_t$ ) is measured while the load is applied and the plastic indentation depth ( $h_p$ ) is measured after complete unloading. Since the unloading curve is fairly linear, and after comparing ABI test results using both complete and partial unloading cycles, ABI tests are now performed with partial unloading (e.g., see Fig. 5). The computer program used to control the test and analyze test data calculates the slope of each unloading cycle and then the intersection of this line with the zero load line (abscissa or X-axis) to determine the value of  $h_p$ . In this work the material-type constant ( $\beta_m$ ) of 0.191 in equation 12 was determined from ABI tests on different stainless steels. The indenter used in this work was machined from hardened 4340 steel. The effect of the surface roughness of this indenter on effective indentation loads was found to be -13%. This was obtained by comparing ABI data using this indenter and another smooth indenter (Rockwell B, 1.59-mm-diam. ball) on A533 grade B class 1 and A212 grade B steels, and type 316L stainless steel. This allowed all yield strength and flow curves results to be adjusted for friction effects. Figures 5 through 7 show ABI test results on type 316L stainless steel base metal. The average ABI-derived yield strength value (305.2 MPa) from three tests (307.5 MPa) from four uniaxial tensile tests. Furthermore, good agreement was obtained between ABI-derived and uniaxial tensile flow properties as shown in Fig. 7.

Figures 8 and 9 show the indentation load-depth curves for the four different aging conditions of the 4% and 12% ferrite 308 SS welds for tests conducted on top of each weld. The results of these ABI flow curves are in agreement with uniaxial tensile properties as shown later and in Ref. 4. A comparison between yield strength values determined from ABI and uniaxial tensile tests is shown in Fig. 10. The dashed lines in this curve represent a  $\pm 5\%$  difference between yield strength values of the nondestructive ABI tests and those from mini-tensile tests conducted on both top and bottom of each weld. Except for one data point (as-welded 4% ferrite) all data from top weld tests fell within the dashed lines. The variation between ABI and tensile results on the bottom of welds were within 16%, possibly because of variation of properties at the bottom of the weld and the fact that

the ABI test is a multiaxial and local test whereas the tensile test is uniaxial and the cylindrical gage section of each mini-tensile test specimen was 3.18 mm in diameter. Although the effect of thermal aging on uniaxial tensile yield strength on the 308 SS welds was small, the ABI results shown in Fig. 11 indicate the same trend. A comparison between yield strength values measured by both tests for top of the weld tests on 12% ferrite aged specimens is shown in Fig. 12.

Furthermore, comparisons between flow properties measured using ABI and uniaxial tensile tests conducted on the top and bottom of 308 SS welds are shown in Figs. 13 and 14. These figures show that the ABI results indicate good agreement with effects of aging. However, the ABI-measured flow curves are about 10-15% higher than those from tensile tests. The ABI tests were conducted at an average strain rate of  $1.8 \times 10^{-3} \text{ s}^{-1}$ , while the strain rate for uniaxial tensile tests was  $3.3 \times 10^{-4} \text{ s}^{-1}$ . Figure 15 shows that the strain rate sensitivity ( $m = 0.079$ ) for the 4% ferrite weld accounts for a 13% higher flow stress at the ABI strain rate. After adjusting the ABI-measured flow curve for such an effect, as explained earlier in equations 6, 8, and 9, good agreement was obtained between ABI and tensile flow curves (Fig. 16). The strain rate sensitivity was not determined for the 8% and 12% ferrite welds; however, their strain rate sensitivity values are expected to be similar to that of the 4% ferrite and could account for the higher ABI flow curves of Figs. 13 and 14.

The yield strength and flow properties of the 4% ferrite weld block were mapped across the thickness of the weld where tests were made near the top, middle, and bottom of the weld. The average ABI-derived yield strength for the base metal, HAZ, and weld materials were 330, 345, and 366 MPa, respectively. All ABI test results showed the expected trend (Fig. 17) of higher flow properties for the weld and HAZ than the base metal. The results of the ABI tests are accurate, repeatable, reproducible, and show excellent agreement with the results from standard tensile tests. Automation of the ball indentation tests makes it accurate, simple, fast (less than 10 minutes per test), and economical (cheaper than a destructive tensile test) for both field and laboratory applications.

## CONCLUSIONS

1. A field indentation microprobe (FIM) was conceived for evaluating the structural integrity of metallic welded components in situ in a nondestructive manner.

2. The laboratory version of the FIM used in this work performed successful automated ball indentation (ABI) tests on as-welded and thermally aged 308 stainless steel welds. Excellent agreement was obtained between yield strength and flow properties measured by both uniaxial tensile and ABI tests.

3. The results also demonstrated that the laboratory ABI technique affords a simple, rapid, accurate, and nondestructive method of determining the flow properties of base metal, HAZ, and welds. Such a technique should be readily adaptable for field applications.

4. The FIM apparatus should be useful in mapping out localized changes in the mechanical and physical properties of welded, deformed, aged, and embrittled structural components.

## ACKNOWLEDGMENT

This work was partially supported by the Office of Nuclear Regulatory Research, Division of Engineering, U.S. Nuclear Regulatory Commission under Interagency Agreement DOE 1886-8011-9B with the U. S. Department of Energy under contract DE-AC-5-84OR21400 with Martin Marietta Energy Systems, Inc. The authors gratefully acknowledge the efforts and help of J. T. Hutton, D. Thomas, and R. L. Swain.

## REFERENCES

1. Haggag, F. M., "Field Indentation Microprobe for Structural Integrity Evaluation," U.S. patent pending, 1988.

2. Haggag, F. M. and Nanstad, R. K., "Estimating Fracture Toughness Using Tension or Ball Indentation Tests and a Modified Critical Strain Model," to be presented at the ASME Pressure Vessel and Piping Conference, Honolulu, July 23-27, 1989, accepted for publication.

3. Haggag, F. M., Nanstad, R. K., and Braski, D. N., "Structural Integrity Evaluation Based on an Innovative Field Indentation Microprobe," to be presented at the ASME Pressure Vessel and Piping Conference, Honolulu, July 23-27, 1989, accepted for publication.

4. Alexander, D. J., Alexander, K. B., and Nanstad, R. K., "The Effect of Aging at 343°C on Type 308 Stainless Steel Welds," to be presented at the 2<sup>nd</sup> International Conference on Trends in Welding Research, Gatlinburg, Tennessee, May 14-18, 1989.

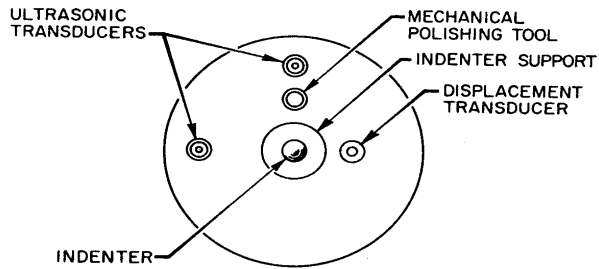
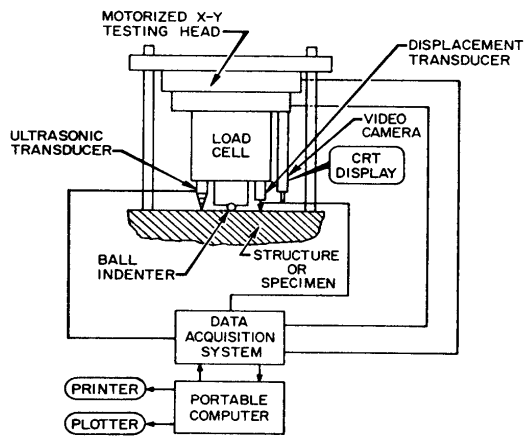


Fig. 1 Basic components of the field indentation microprobe (FIM) apparatus. (a) Schematic and block diagram, (b) relative positions of the testing tools mounted on the bottom of the load cell of the FIM apparatus.

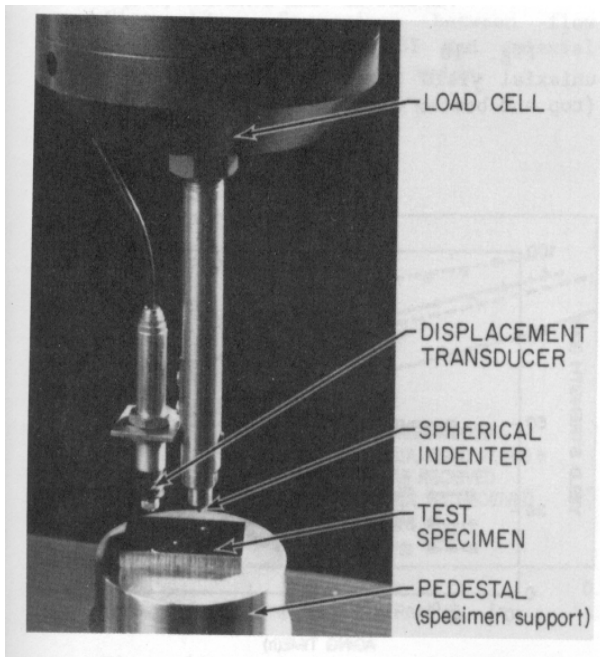


Fig. 2 Ball indenter and spring-loaded LVDT mounted to the load cell of a hydraulic testing machine (not shown in figure).

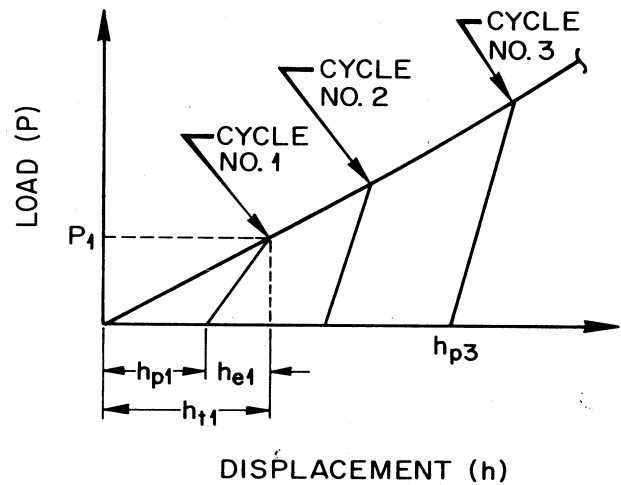


Fig. 3 Schematic representation of the relationship between load and displacement of the ball indenter of Fig. 2 as observed by increased cyclic loading.

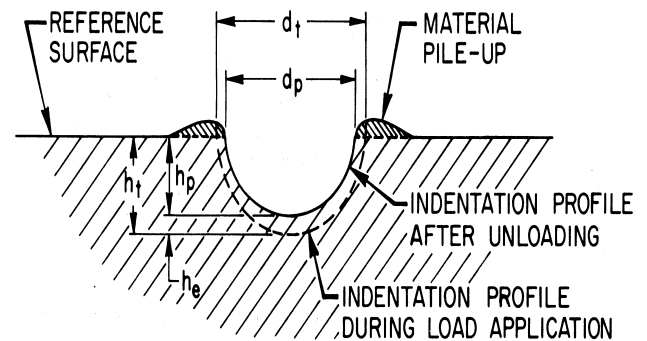


Fig. 4 Illustration of indentation geometries before and after load application (the material pile-up around the indentation is exaggerated).

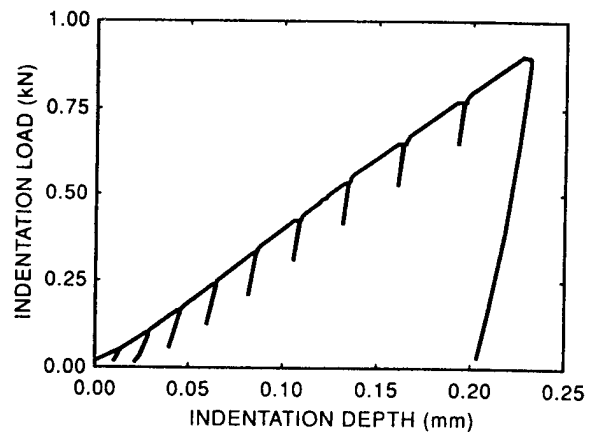


Fig. 5 Samples of ABI test results (load versus depth using a 0.76-mm-diam ball indenter) on 316L stainless steel (SS) base metal.

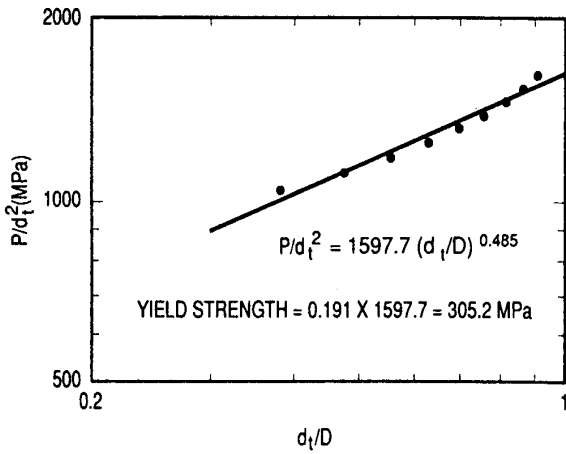


Fig. 6 Yield strength results calculated from the entire ABI load-depth curve of Fig. 5 for 316L SS specimen.

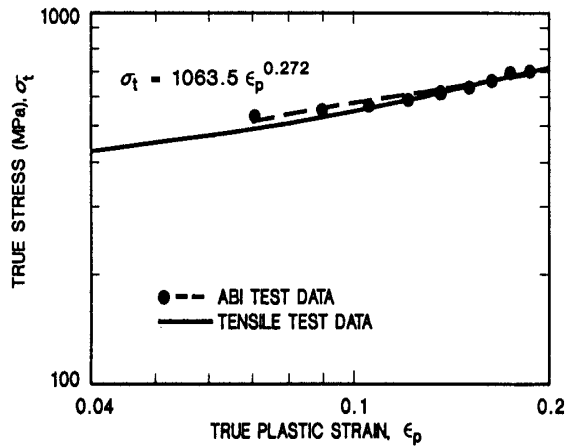


Fig. 7 Comparison between flow properties (true-stress/true-plastic-strain curve) measured from ABI and uniaxial tensile tests on 316L stainless steel. (note that the ABI curve is entirely obtained from multiple indentations at a single penetration location.)

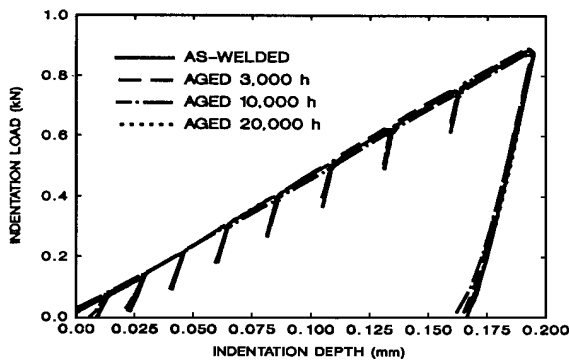


Fig. 8 Effect of thermal aging on ABI test results of 308 SS welds with a 4% delta ferrite (top of weld data).

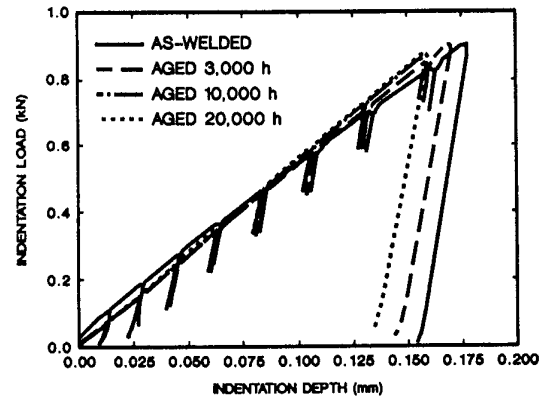


Fig. 9 Effect of thermal aging on ABI test results of 308 SS welds with a 12% delta ferrite (top of weld data).

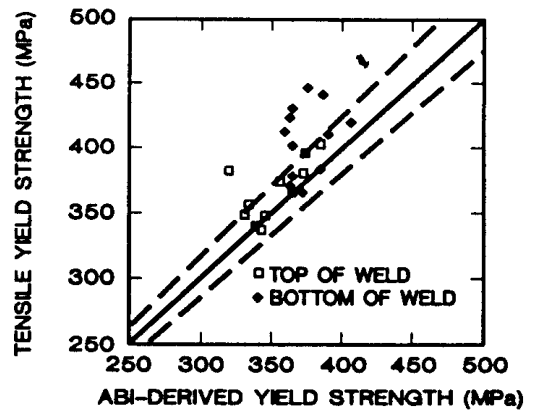


Fig. 10 Comparison between ABI and uniaxial yield strength values for 12 welds (top and bottom weld data).

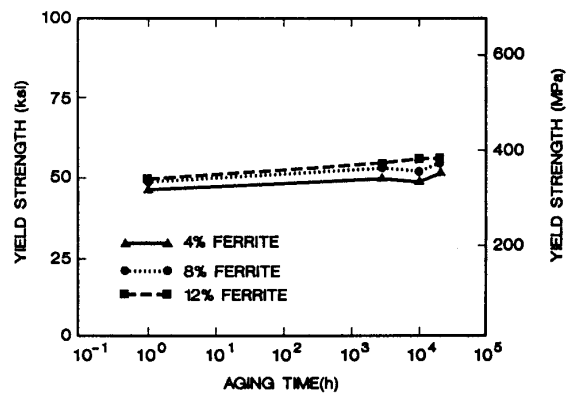


Fig. 11 Effect of thermal aging on the ABI-derived yield strength for 308 SS welds (top of weld data).

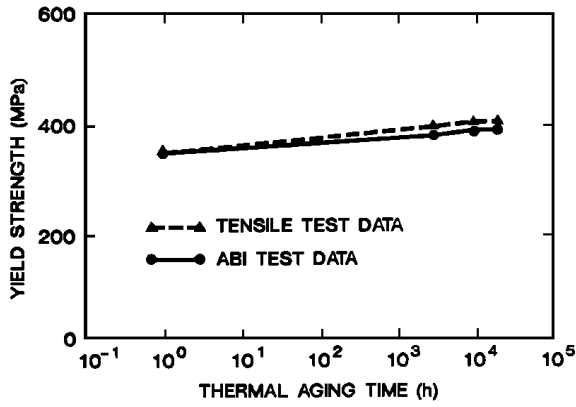


Fig. 12 Comparison between yield strength values measured from ABI and uniaxial tensile tests on top of 308 SS welds.

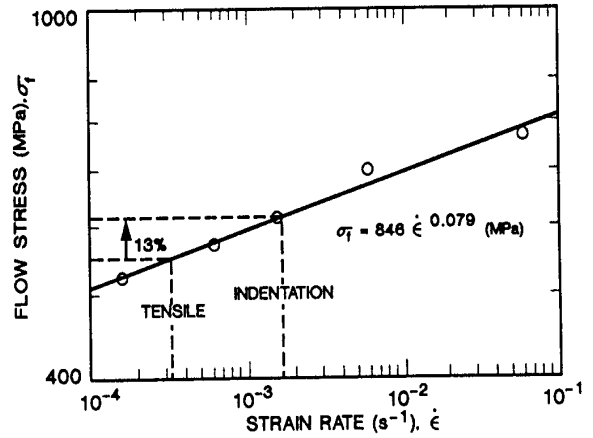


Fig. 15 Relationship between flow stress and strain rate for as-received 308 SS weld containing 4% delta ferrite.

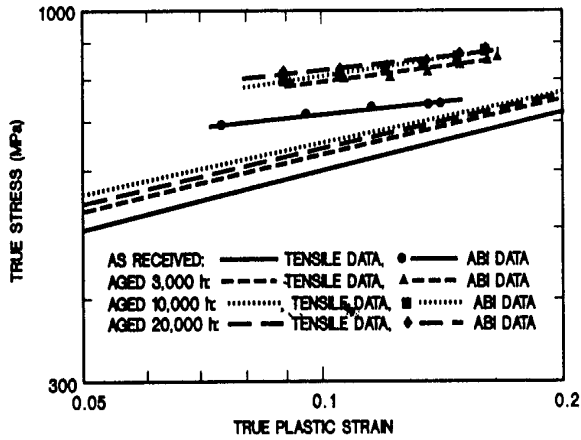


Fig. 13 Comparison between flow properties measured using ABI and uniaxial tensile tests on top of 308 SS welds.

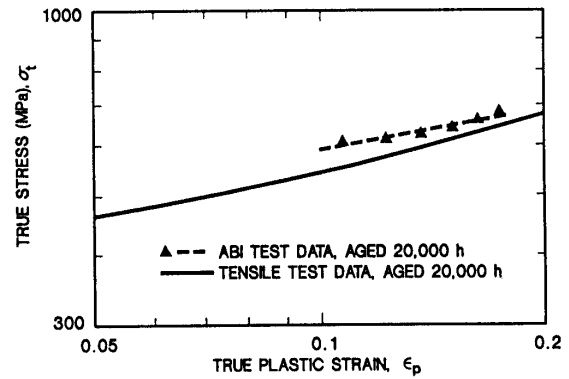


Fig. 16 Comparison between flow properties measured from ABI and uniaxial tensile tests on top of 308 SS weld after adjusting ABI data for strain rate sensitivity.

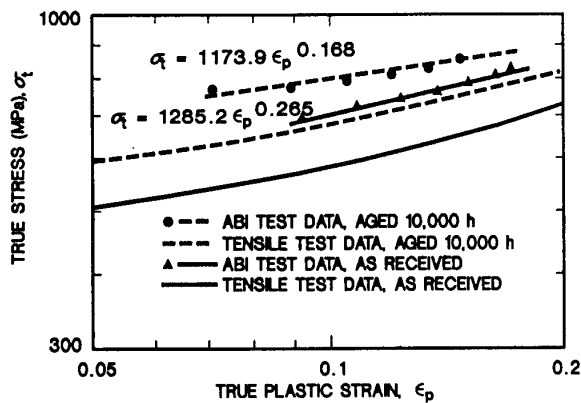


Fig. 14 Comparison between flow properties measured from ABI and uniaxial tensile tests conducted on bottom of 308 SS welds.

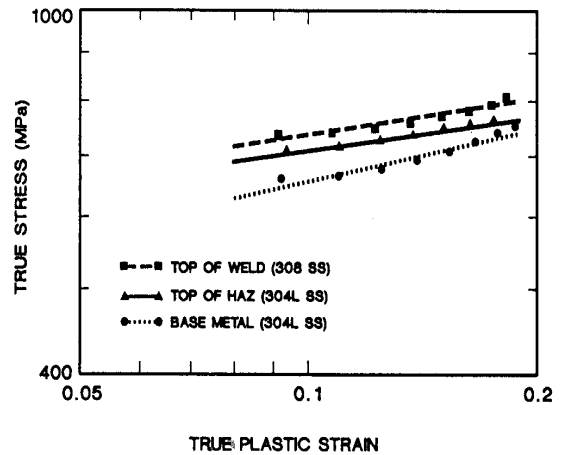


Fig. 17 Comparison between flow properties measured from ABI tests conducted on 304L SS base metal, heat affected zone (HAZ), and 308 SS weld.